JACS
JOURNAL OF THE AMERICAN CHEMICAL SOCIETY
Article
pubs.acs.org/JACS

Visualizing The Enhanced Chemical Reactivity of Mesoporous Ceria; Simulating Templated Crystallization in Silica Scaffolds at the Atomic Level

Thi X. T. Sayle and Dean C. Sayle*

School of Physical Sciences, University of Kent, Canterbury, CT2 7NZ, United Kingdom

ABSTRACT: Unique physical, chemical, and mechanical properties can be engineered into functional nanomaterials via structural control. However, as the hierarchical structural complexity of a nanomaterial increases, so do the challenges associated with generating atomistic models, which are sufficiently realistic that they can be interrogated to reliably predict properties and processes. The structural complexity of a functional nanomaterial necessarily emanates during synthesis. Accordingly, to capture such complexity, we have simulated each step in the synthetic protocol. Specifically, atomistic models of mesoporous ceria were generated by simulating the infusion and confined crystallization of ceria in a mesoporous silica scaffold. After removing the scaffold, the chemical reactivity of the templated mesoporous ceria was calculated and predicted to be more reactive compared to mesoporous ceria generated without template; visual "reactivity fingerprints" are presented. The strategy affords a general method for generating atomistic models, with hierarchical structural complexity, which can be used to predict a variety of properties and processes enabling the nanoscale design of functional materials.

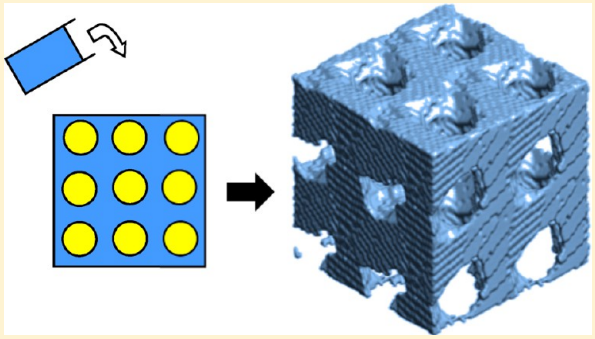

INTRODUCTION

The properties of contemporary functional nanomaterials, are critically dependent upon their hierarchical structural complexity, which span multiple length scales, including: crystal structure, microstructure, such as grain-boundaries, dislocations intrinsic/extrinsic point defects, and nanoarchitecture, including particles (0D), rods (1D), sheets (2D), and mesoporous (3D). (The architecture of the mesoporous material includes, for example, the space symmetry and connectivity of the internal channel/pore network, the curvature and morphology (surfaces exposed) of the internal pores of the mesoporous material.) The origins of such structural complexity rest with the synthetic protocols used for their fabrication, which exploit a diverse range of innovative and inter-related strategies. These include, for example, self-assembly,[1] oriented attachment,[2,3] and templating using soft, hard, and even bioinspired scaffolds;[4] a review is given in ref 5. Computer simulation has, for over forty years, provided unique complementary insight and prediction for experiment. However, if atomistic models are to be generated and then interrogated to reliably predict the properties of functional nanomaterials for experiment, all these (synergistic) levels of structural complexity must be captured within a single atomistic model. For example, if one wished to interrogate an atomistic model to calculate mechanical properties, the results could be orders of magnitude in error if the model did not include dislocations.

Atomistic models are normally generated using symmetry operators.[6] However, the challenge to generate models with the hierarchical structural complexity of contemporary functional nanomaterials may soon prove insurmountable using such strategies. In particular, atomistic simulation codes are available to generate an atomistic model of a crystal, such as CeO_2, which includes an isolated dislocation or a grain-boundary.[7] However, methods for generating models of mesoporous materials, which comprise interconnecting networks of channels, are less widely reported in the open literature.[8] Challenges include, for example: determining the surfaces exposed at the internal channels; how the surfaces facilitate (convex and concave) channel curvature; the orientation of the crystal structure with respect to the direction of the network of pores or space symmetry of the mesoporous architecture; microstructural features, such as dislocations, grain-boundaries, and point defects within the framework material. And while a particular dislocation or grain-boundary might be (energetically) stable within the parent bulk material, would it also be stable within the walls of the mesoporous material, which may only be 10 nm thick?

Intuitively, the best way to generate atomistic models is to simulate directly their experimental method of fabrication. Here, we undertake such a strategy and generate atomistic models of mesoporous ceria by simulating, at the atomistic level, the confined crystallization of mesoporous ceria using a silica template. The model is then interrogated to predict its catalytic properties.

Received: January 15, 2014
Published: February 17, 2014

   dx.doi.org/10.1021/ja500443m | J. Am. Chem. Soc. 2014, 136, 4056−4065

The synthetic protocol that we have chosen to simulate is that of Ji and co-workers, who fabricated mesoporous ceria by infusing ceria into a mesoporous silica template (MCM-48) and crystallizing at high temperature.[9] The silica template was then removed and the reactivity of the templated mesoporous ceria measured. Here, we mirror each step in the synthesis at the atomistic level using Molecular Dynamics (MD) simulation to generate an atomistic model for mesoporous ceria and use the model to predict the reactivity of the functional material.

We have chosen ceria as a model system because it is exploited in a diverse range of important applications, owing to its remarkable properties. Moreover, published data on nanostructured ceria shows that the properties of the material are influenced profoundly by its hierarchical structural complexity. For example, its high oxygen storage capacity enables the material to extract, store and liberate oxygen, which is widely exploited in (oxidative) catalysis and pollutant mitigation.[10] This can be attributed to the morphology of the mesoporous ceria, which can be modified (via the synthetic protocol) to facilitate a profound increase in reactivity. Specifically, nanoparticles and nanorods can be synthesized to proffer reactive $CeO_2\{100\}$ surfaces, rather than the thermodynamically more stable, but less reactive $CeO_2\{111\}$ surfaces.[11,12] Atomistic simulation showed that the increased reactivity is because oxygen is more easily extracted from $CeO_2\{100\}$ and $CeO_2\{110\}$ surfaces compared to $CeO_2\{111\}$ surfaces.[13,14] The increased reactivity of nanoceria has also been exploited in the field of nanomedicine. Here, by carefully controlling the morphology (surfaces exposed) and size of ceria particles, one is able to modulate oxygen concentrations in biological environments;[15] ceria nanoparticles are also able to scavenge reactive oxygen species.[16] In particular, ceria nanoparticles can act like crystalline inorganic "molecules",[17] which are able to traverse biological environments to store and release oxygen at targeted locations.

The ability of ceria to sustain high levels of reduction and accommodate dopant ions, such as Gd^{3+}, at lattice positions while retaining the fluorite structure of the fully oxidized parent material, enables application in solid oxide fuel cells.[18] This is because metal^{3+} species facilitate oxygen vacancies to ensure charge neutrality. Oxygen ions are then able to diffuse, driven via a vacancy mechanism, through the host ceria lattice. The microstructure is pivotal to such diffusion: point defects,[19] grain-boundaries,[20] and dislocations[21] have all been shown to significantly enhance or inhibit ionic mobility. More recently, the strain within a nanomaterial has been hotly debated as a potential driver for enhanced ionic mobility[18] and also impacts upon the reactivity[22] and optical and electronic properties of a nanomaterial.[23] Strain can be engineered into the system by interfacing nanoceria with a lattice mismatched substrate;[18,24] surface relaxation, associated with the nano form of ceria, also induces localized strain within the lattice, as does the complex microstructure, which evolves in an attempt to help quench the strain. This system[18] epitomises a structurally complex nanomaterial where each hierarchical level of structural complexity impacts synergistically upon its properties. Such evidence drives the need for atomistic models of nanomaterials, which include hierarchical structural complexity to enable reliable property prediction for experiment. A review of the synthesis, properties, and applications of nanostructured ceria is given by Sun.[25]

METHODS

In this section, we detail the potential model used to describe mesoporous ceria and silica template, the computer code used to perform the molecular dynamical simulations and the approach used to simulate each synthetic step associated with the synthesis of real mesoporous ceria.

Potential Model. All calculations presented in this study were based upon the Born model of the ionic solid, where the energy, E, of the system is given by the following:

$$E(r_{ij}) = \sum_{ij} \frac{Q_i Q_j}{4\pi\varepsilon_o r_{ij}} + \sum_{ij} A \exp\left(\frac{-r_{ij}}{\rho}\right) - C r_{ij}^{-6}$$

the first term represents the Coulombic interaction between ion i of charge Q_i and ion j of charge Q_j, which are a distance r_{ij} apart. The second term is of the Buckingham form, which is particularly effective in representing ionic solids. Model parameters, used to describe SiO_2 and CeO_2 are presented in table 1 and were taken from: ref [26 and 13]

Table 1. Interionic Potential Parameters, of the Buckingham Form: $E(r_{ij}) = \Sigma_{ij}(Q_iQ_j)/(4\pi\varepsilon_o r_{ij}) + \Sigma_{ij}A \exp((-r_{ij})/\rho) - Cr_{ij}^{-6}$, and Three Body Potential: $E(\theta) = 1/2K(\theta_o - \theta)^2$, Used to Describe the SiO_2 and CeO_2

Buckingham	A (Å)	ρ (Å)	C (eV. Å^6)
$O^{2-}-O^{2-}$	22764.300	0.149	27.89
$Si^{4+}-O^{2-}$	1283.907	0.302	10.66
$Ce^{4+}-O^{2-}$	1986.300	0.351	20.40
three body	K (eVrad^{-2})	θ_o (deg)	
O−Si−O	2.09724	109.47	

Simulation Code. All the molecular dynamics simulations (MD) were performed using the DL_POLY code.[27] The user manual provides comprehensive analytical descriptions and discussion of the molecular dynamics simulations, force fields, boundary conditions, algorithms, and parallelization methods used in these simulations; three-dimensional periodic boundary conditions were imposed throughout.

Generating Atomistic Models. The underpinning strategy used to mirror experiment, is detailed below:

Step 1. Generate mesoporous silica template.

Step 2. Infuse ceria into the void space of the template.

Step 3. Crystallize the infused ceria within the confined environment of the silica template.

Step 4. Remove the silica template.

Step 5. Calculate chemical reactivity of mesoporous ceria.

A schematic of the procedure is shown in Figure 1. The simulations mirror the fabrication of the silica scaffold described in ref 28 and the templated crystallization of ceria using the silica scaffold described in ref 9.

STEP 1. Generate Silica Template.

Experiment. "Silica molecular sieves MCM-48 were prepared in aqueous solution using CTAB and TEOS, following ref 28".

Simulation. Mesoporous silica with P1 (plumbers nightmare) symmetry was generated by positioning amorphous SiO_2 nanoparticles, comprising 24 696 atoms, at cubic lattice positions. The nanoparticles were then agglomerated with their periodic neighbors, using MD simulation, to facilitate a mesoporous structure.[8]

STEP 2. Infuse Ceria into Silica Template.

Experiment. A 2.5-g portion of $Ce(NO_3)_3{\cdot}6H_2O$ was dissolved in 20 mL of absolute ethanol. To this solution, 0.5 g MCM-48 was dispersed and heated at 333 K under vigorous stirring; after the ethanol had evaporated, the system was heated at 723 K and the process repeated with an ethanol solution of 1.2 g $Ce(NO_3)_3{\cdot}6H_2O$.

Simulation. The infusion process was simulated by introducing amorphous ceria into the void space within the silica template. In particular, amorphous CeO_2 nanoparticles, comprising 15 972 atoms,

dx.doi.org/10.1021/ja500443m | J. Am. Chem. Soc. 2014, 136, 4056−4065

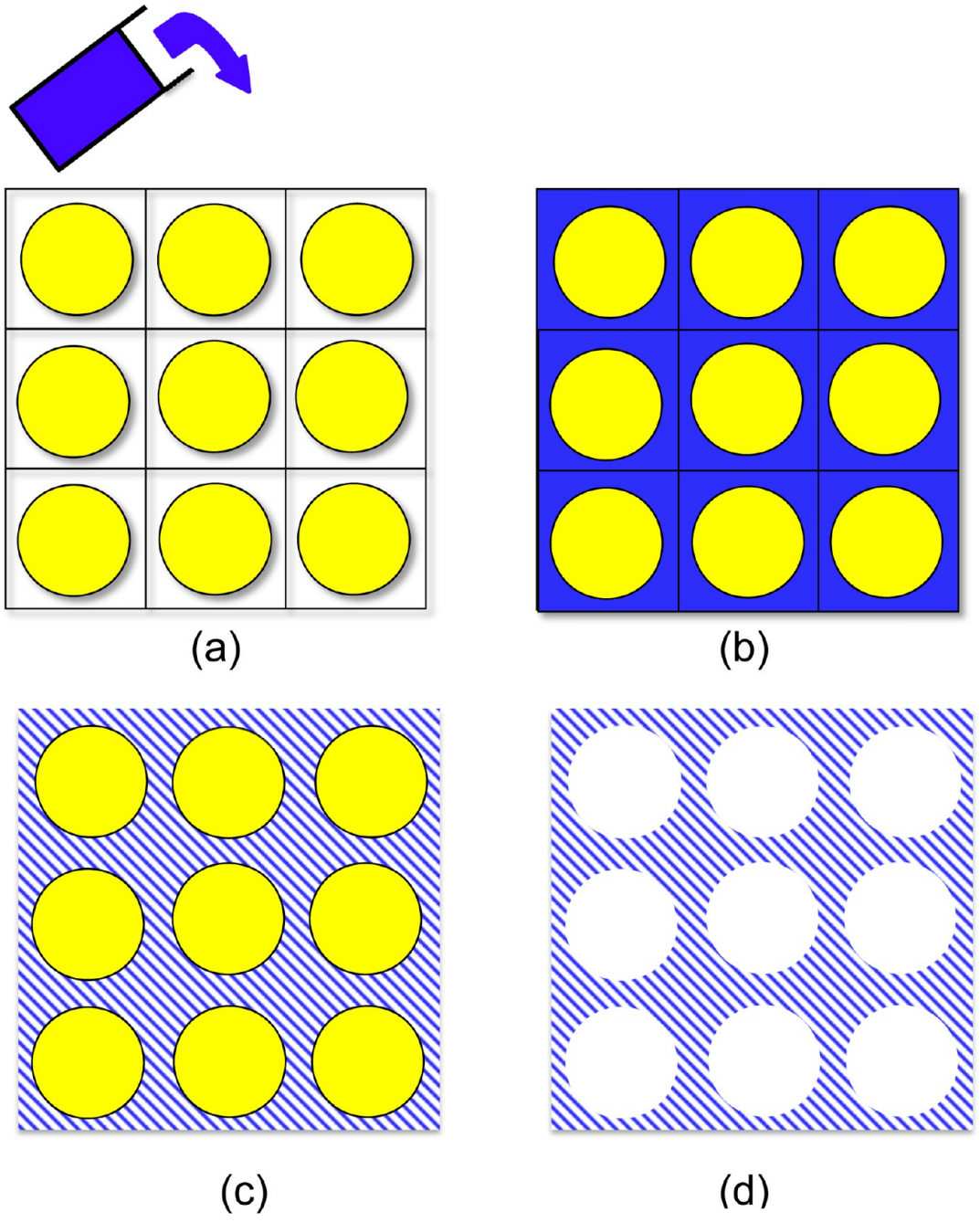

Figure 1. Schematic describing the templating procedure. (a) Generation of the silica template (colored yellow). (b) Infusion of ceria (colored blue) into the pore space of the silica template. (c) Crystallization of the ceria within the silica pores. (d) Mesoporous ceria after removal of the silica template.

were placed within the void space of the model silica template. The nanoparticles were compressed by 70% such that under MD simulation, they would expand to fill the void within the mesoporous silica under MD simulation. The silica template was held fixed and NVT simulation performed at 2800 K until the (amorphous) ceria completely filled the internal void space of the silica template.

Molecular graphical images depicting the infusion of ceria into the pore space of the silica template are shown in Figure 2(a–g); the images represent atom positions comprising the SiO_2 host and template CeO_2 and are not schematics.

STEP 3. Crystallize the Amorphous Ceria.

Experiment. The cerium precursor/silica composite was calcined at 873 K to crystallize the ceria networks inside the silica template.

Simulation. The ceria was crystallized inside the silica host template by performing NVT simulation for 3 ns at 2800 K with a 0.002 ps time step; the silica template was held fixed to prevent intermixing of the Si and Ce cations. The duration of the simulation was sufficient to crystallize the ceria fully, Figure 3. The system was then cooled to 1 K by performing NVT simulation at 1 K for 20 ps using a 0.002 ps time step.

STEP 4. Remove Template.

Experiment. The silica template was removed by treating three times with 2 M NaOH solution at 60 °C for 10 min each time.

Simulation. The silica host was removed by "deleting" the Si_iO atoms from the simulation cell and any residual stress in the mesporous ceria eliminated by performing NPT simulation at 1 K for 16 ps.

STEP 5. Surface Reactivity.

Experiment. Oxidation of acid orange 7 using the mesoporous ceria and visible light was monitored.

dx.doi.org/10.1021/ja500443m | J. Am. Chem. Soc. 2014, 136, 4056–4065

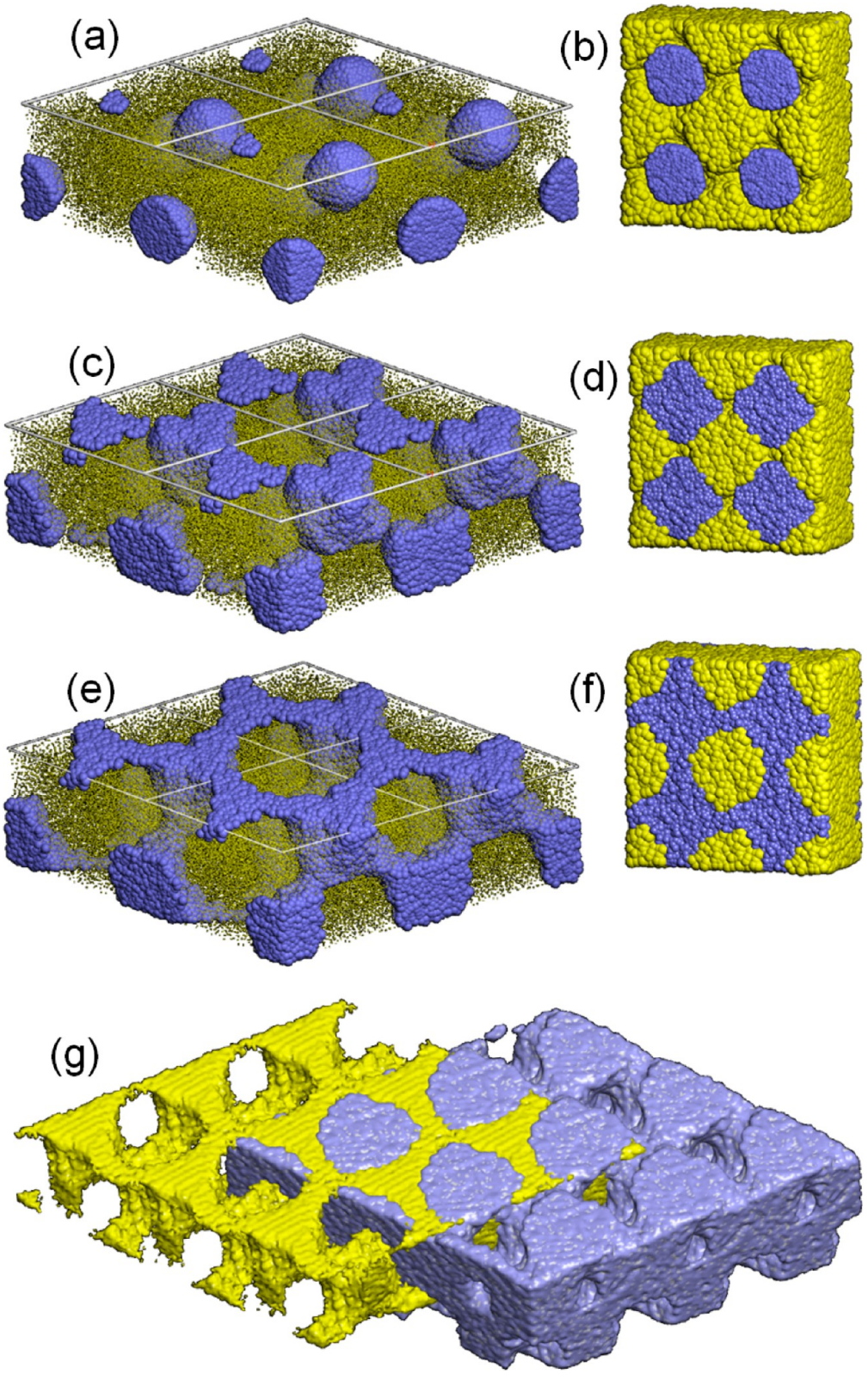

Figure 2. Atomistic models depicting the simulated infusion of ceria in a silica template. (a) Nanoparticles of ceria positioned within the void space of the mesoporous silica; (b) slice cut through the system showing more clearly the nanoparticles inside the silica template; (c) infusion of the ceria, which starts to fill the cavities and connecting channels of the silica template; (d) slice cut through (c); (e) complete infusion of the ceria filling all the pore space of the template; (f) slice cut through (e); (g) perspective view of a surface rendered model showing more clearly the infusion of ceria into the host silica template. Silicon and cerium atom positions are represented by yellow and blue spheres, respectively; oxygen atom positions are not shown to improve clarity of the figures. The silicon atom positions in (a), (c), and (e) are represented by small spheres to improve clarity enabling visualization of the infusing ceria.

dx.doi.org/10.1021/ja500443m | *J. Am. Chem. Soc.* 2014, 136, 4056−4065

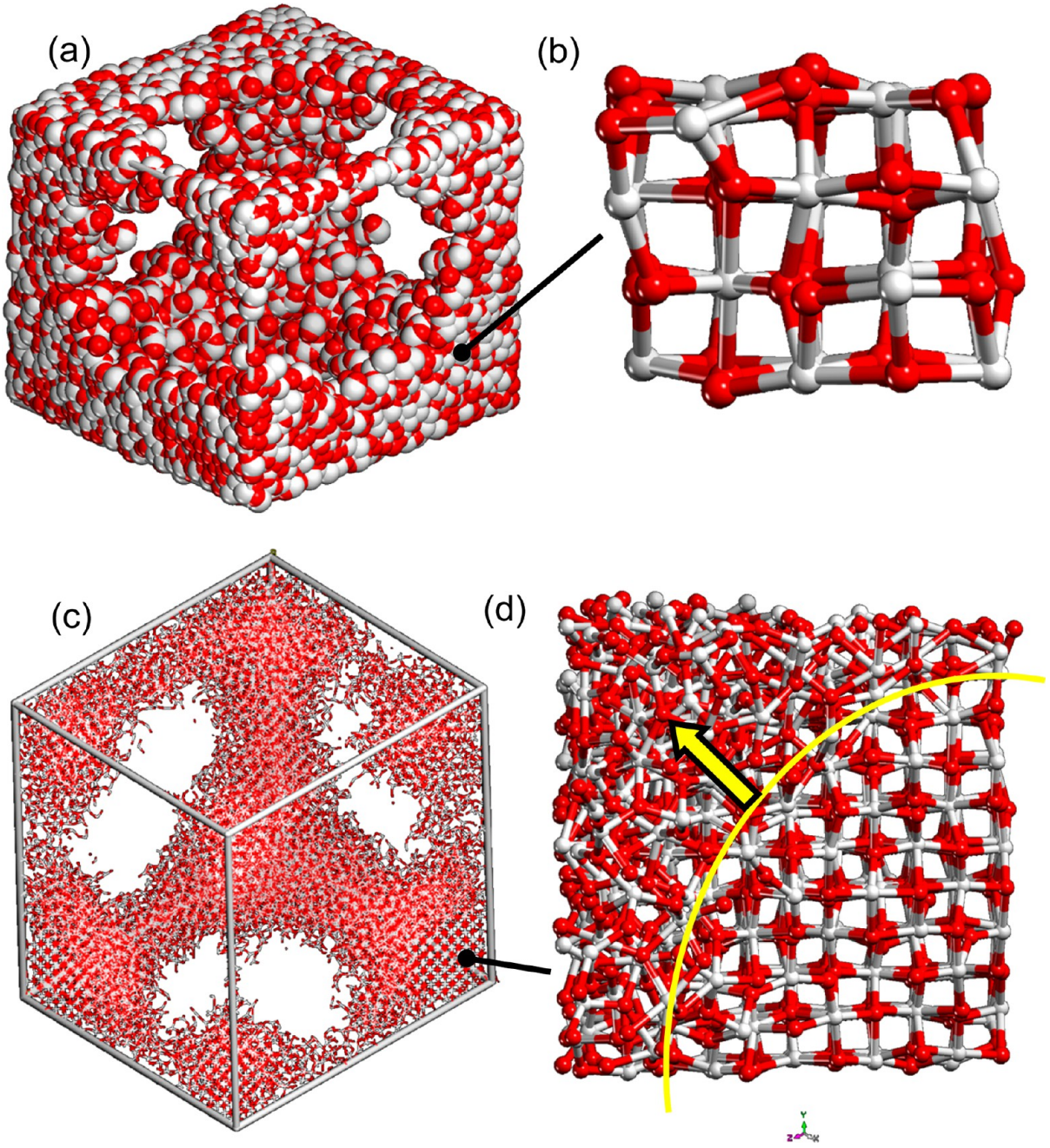

Figure 3. Atomistic models depicting the crystallization of ceria infused into the silica template; the silica template is not shown to ensure clarity. (a) Sphere model representation of the Ce (white) and O (red) atoms after a fluorite-structured crystalline seed, shown in (b), had spontaneously evolved within the ceria lattice. (c) A snaphot taken during the crystallization process showing that the seed has started to nucleate the crystallization of the ceria framework. (d) Segment of the mesoporous ceria, shown in (c), with crystalline and amorphous regions. The crystallization front is shown as the yellow curve on the figure with the crystallization front moving in the direction of the arrow and emanating radially from the nucleating seed.

Simulation. Surface reactivity of the mesoporous ceria was determined by calculating the electrostatic potential of surface oxygen species. In particular, the electrostatic potential correlates with how strongly oxygen is bound to the internal surfaces of the mesoporous ceria and is therefore indicative of its surface reactivity.[22]

The method for generating a model of mesoporous ceria without template is presented in ref 29.

RESULTS

In this section, we explore the infusion of ceria into the mesoporous silica template, the (confined) crystallization of the ceria in the template, the removal of the template and finally the reactivity of templated compared to untemplated ceria.

Ceria Infusion. Figure 2(a,b) show the ceria nanoparticles positioned within the cavities of the mesoporous silica. Snapshots of the system, taken during the MD simulation, reveal the infusion of the ceria nanoparticles into the cavities and channel network (with three-dimensional connectivity) within the silica template, Figure 2(c,d). Finally, the neighboring ceria nanoparticles coalesce to facilitate a fully interconnected mesoporous ceria, Figure 2(e,f). We note that the structure of the infused ceria adopts the shape and

dx.doi.org/10.1021/ja500443m | J. Am. Chem. Soc. 2014, 136, 4056−4065

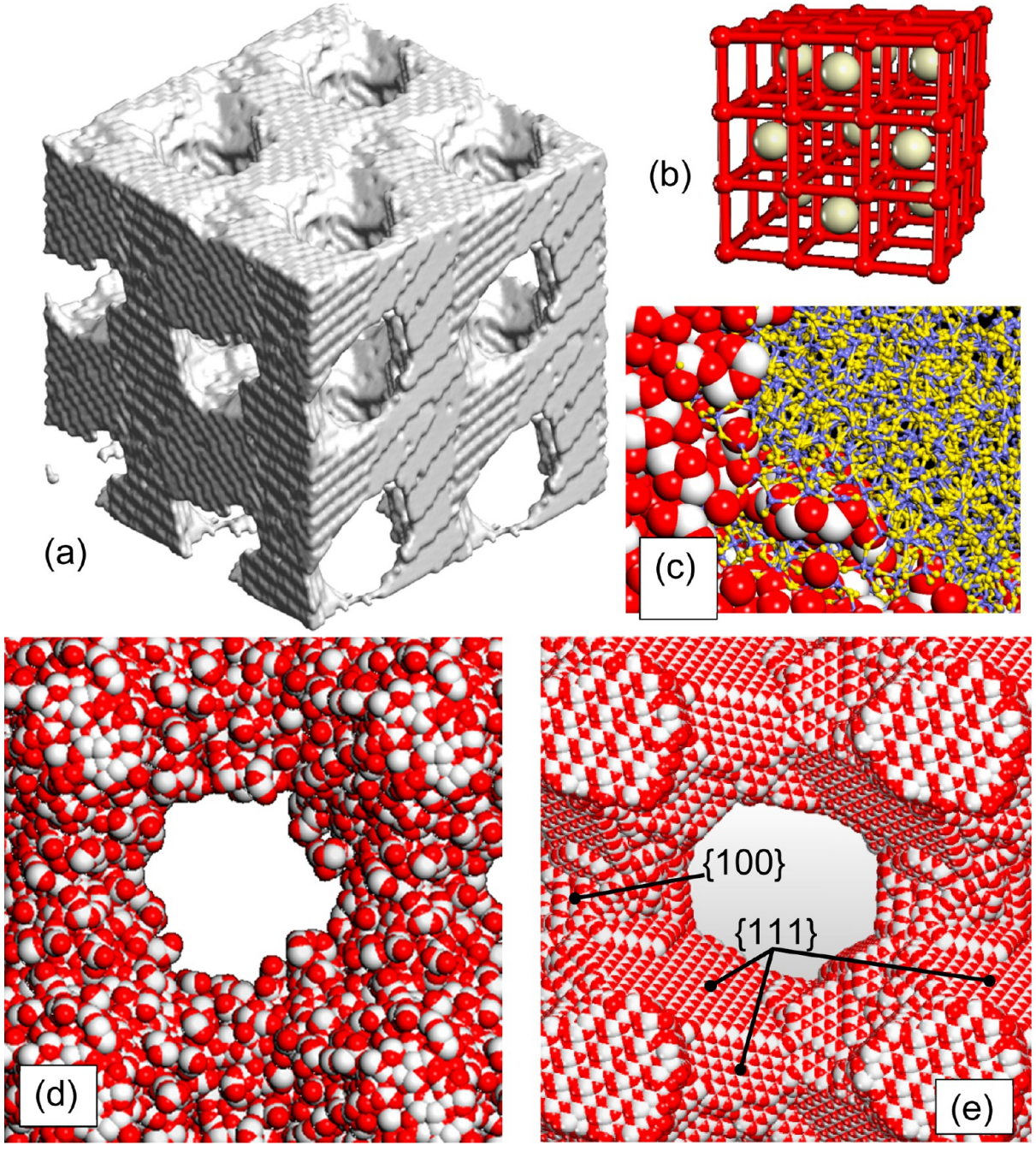

Figure 4. Atomistic models of the crystallized mesoporous ceria. (a) Surface rendered model of the templated mesoporous ceria showing the network of channels, which traverse three-dimensions. (b) A segment of (a) revealing that the crystalline CeO_2 conforms to the fluorite structure. (c) Segment cut through the simulation cell, showing the templated ceria and silica template, revealing that the silica template inhibits the evolution of CeO_2{111} at the internal pore surfaces. (d) Final, low temperature structure looking through one of the channels in the templated mesoporous ceria after the silica template has been removed, revealing no obvious faceting of the internal walls of the ceria. (e) View looking along one of the channels in a model of mesoporous ceria generated without template showing clearly the highly {111}-faceted walls. Cerium is colored white, oxygen (CeO_2) is red, silicon is blue, and oxygen (SiO_2) is yellow.

connectivity of the network of pores within the SiO_2 template, Figure 2(g).

Crystallization. Snapshots of the model ceria structure, taken during the simulated crystallization step, reveal that a crystalline seed, conforming to the fluorite structure, Figure 3(a,b), spontaneously evolves within the amorphous sea of ions and nucleates the crystallization of the templated ceria. The crystalline seed then nucleates crystallization of the remaining amorphous Ce,O ions, emanating radially from the seed until all the ceria is crystalline, Figure 3(d).

The final, low temperature model structure for templated mesoporous ceria is shown in Figure 4 and reveals an interconnected network of pores, which traverse three-dimensions, Figure 4(a); the mesoporous ceria conforms to the fluorite structure, Figure 4(b).

Analysis of the internal pores of the atomistic model using graphical techniques reveals that they are not faceted, exposing,

dx.doi.org/10.1021/ja500443m | J. Am. Chem. Soc. 2014, 136, 4056−4065

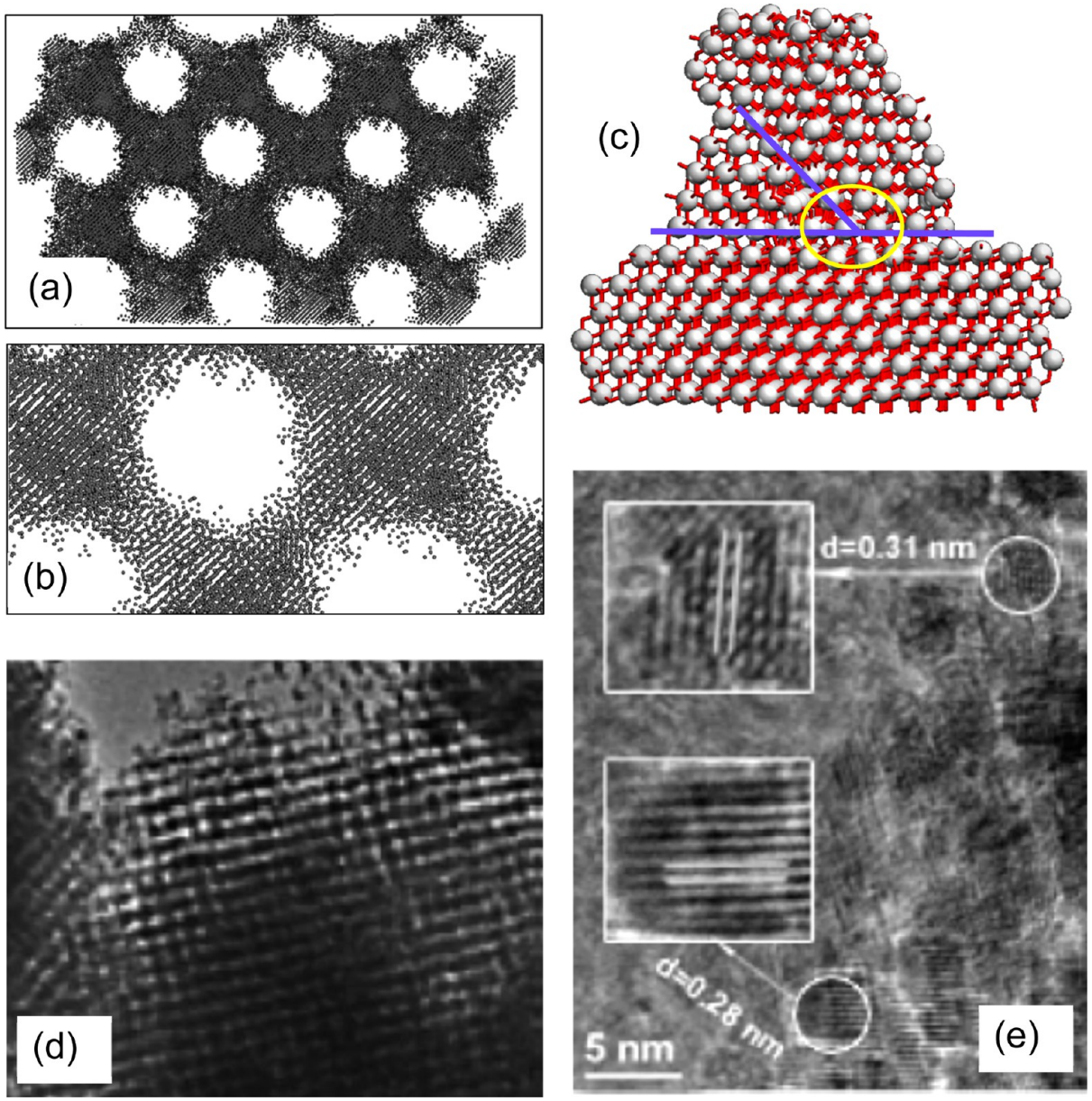

Figure 5. Atomistic model of mesoporous ceria showing the pore structure compared with experiment. (a) Sphere model representation of the cerium atom positions (oxygen positions not shown) comprising mesoporous ceria. (b) Enlarged segment of (a) showing more clearly the atomic planes and crystallinity of the mesoporous ceria. (c) Atom positions comprising a segment of the ceria wall showing the crystalline structure together with grain-boundaries and triple junction (circle) highlighted by the blue lines; straight lines are somewhat disingenuous because the grain-boundaries are in reality curved and twisted, rather the lines provide a visual guide. Cerium atom positions are represented by the gray spheres and oxygen atom positions are shown as the red sticks connected to the ceria atoms. (d) and (e) HRTEM images of mesoporous ceria to compare, taken with permission from ref 9; copyright 2008, American Chemical Society.

for example, $CeO_2\{111\}$ surfaces; rather the confining influence of the amorphous SiO_2 template, together with CeO_2−SiO_2 interfacial interactions, prevents evolution of (planar) $CeO_2\{111\}$ surfaces at the interface, Figure 4(c). Consequently, the embryonic crystalline seed evolves "deep" within the wall of the ceria, Figure 3(c), rather than at the surface because there is no space available to facilitate evolution of a seed exposing {111} at the pore surface.

A view looking along one of the channels in SiO_2-templated mesoporous ceria is shown in Figure 4(d) and is compared to mesoporous ceria generated without template, Figure 4(e). The latter comprises highly faceted pores exposing predominantly $CeO_2\{111\}$ and small domains of $CeO_2\{100\}$ together with steps, edges, and corners to help navigate the channel. The nucleating seed for the latter structure, Figure 4(e), was able to spontaneously evolve on the surface exposing $CeO_2\{111\}$ because it was not confined by the SiO_2 template.

The atomistic model of mesoporous ceria is compared to experiment in Figure 5. In particular, Figure 5(a) shows a slice cut through the templated mesoporous model revealing the channels, which are shown enlarged in Figure 5(b); a TEM image of mesoporous CeO_2 is shown in Figure 5(d,e). Inspection of the TEM images reveals that the mesoporous ceria comprises crystalline grains about 5 nm in diameter. Molecular graphics was used to explore whether the model of mesoporous ceria also comprised similar grains separated by

dx.doi.org/10.1021/ja500443m | J. Am. Chem. Soc. 2014, 136, 4056−4065

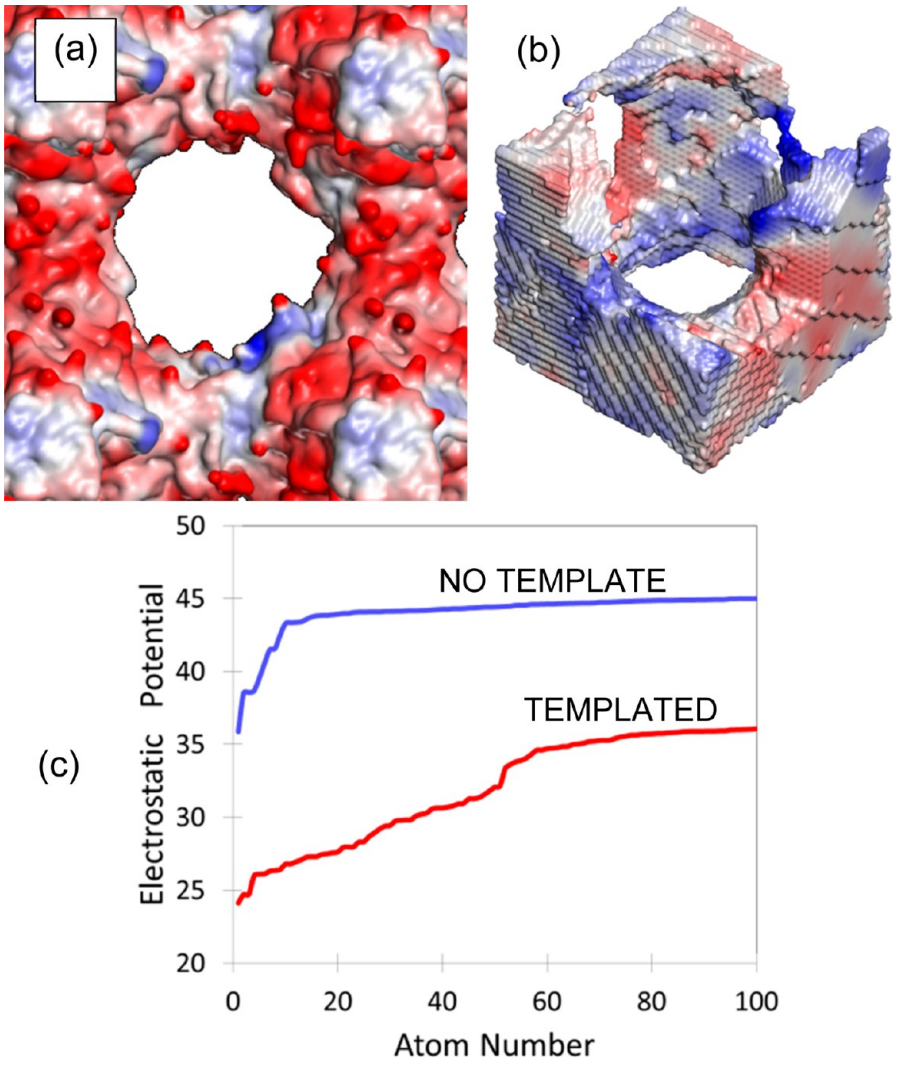

Figure 6. Reactivity "fingerprints" calculated for mesoporous ceria models. (a) Surface rendered model of mesoporous ceria generated using a silica template with the surface oxygen ions colored according to electrostatic energy. (b) Surface rendered model of mesoporous ceria, generated without template, with the surface oxygen ions colored according to electrostatic energy. (c) Calculated electrostatic potential of surface oxygens comprising the templated, (a), and nontemplated, (b), mesoporous ceria models; only the most active (lowest electrostatic potential) 200 surface oxygen species are shown. The reactivity is show via a red-white-blue gradiented scale; regions colored red are indicative of high reactivity (easy to extract surface oxygen), and regions colored blue are indicative of low reactivity (tightly bound oxygen ions and therefore difficult to extract).

grain-boundaries. A segment cut from the mesoporous structure is shown in Figure 5(c) and reveals missoriented grains, grain-boundaries, and triple junction. Our models are therefore commensurate with the real material, which comprises nanocrystalline grains about 5 nm in diameter, Figure 5(d,e).

Reactivity. It is pertinent to question whether templated mesoporous ceria exhibits different reactivity compared to the mesoporous ceria generated without silica scaffold. A key indicator for the reactivity of ceria is its ability to store and release oxygen and therefore act catalytically in oxidation/reduction reactions. The oxidative catalytic reactivity rests intuitively on the ease (energy) of extraction of surface oxygen to participate in an oxidation reaction, which is governed by how strongly oxygen is bound to the surface of the ceria catalyst. Previously, we showed that this reactivity can be gauged by calculating the electrostatic potential of the surface oxygen ions.[22] Accordingly, to gauge surface reactivity, the electrostatic potentials of the surface oxygens were calculated for templated mesoporous ceria compared to mesoporous ceria, which was generated without template. The oxygen atoms at the surface of the internal pores, colored according to electrostatic potential, are shown in Figure 6. The images therefore reveal visual "fingerprints" of the surface reactivity of the mesoporous materials.

Inspection of the reactivity maps reveals that surface oxygen is loosely bound to the templated crystalline mesoporous ceria, Figure 6(a), as evidenced by the wealth of red coloration of the model. Conversely, for the nontemplated and predominantly {111}-faceted mesoporous ceria model, the red coloration is less prevalent indicating that it is more difficult to extract surface oxygen and hence potentially less active. This is attributed to the planar CeO_2{111} surfaces, which bind the oxygen tighter to the structure.

The electrostatic potential, calculated for surface oxygens with the lowest electrostatic potentials, are shown in Figure 6(c). Inspection of the figure reveals a marked enhanced reactivity for the templated mesoporous ceria compared to mesoporous ceria generated without template.

dx.doi.org/10.1021/ja500443m | J. Am. Chem. Soc. 2014, 136, 4056−4065

DISCUSSION

The key difference between models generated with and without template is the constrained crystallization of the MCM-48 templated ceria compared to unconstrained crystallization of the ceria generated without template.

For example, the first few layers of a thin-film deposited on a crystalline substrate can adopt the configuration of the substrate; epitaxial constraints drive the structural evolution.[30] Moreover, the substrate can be carefully chosen to tune the properties of the thin-film via structural control.[31] However, the "field of thin-films" manifest as a special 2D case of a more generate 3D phenomenon—that of nanoporous templating. There are a variety of methods used to fabricate mesoporous materials, including soft (surfactant, polymer, biopolymer) or hard (Silica) templating.[4] For each of these methods, the template directs, via epitaxy and confinement, the structure of the templated material and although the surface area, porous structures and Ce/O ratio might be commensurate for mesoporous materials generated using different (hard, soft) templates, it is the atomistic structure of the surfaces exposed at the internal pores that governs the reactivity. In particular, it is the particular template, which directs the evolution of the (internal) surfaces and hence the reactivity. Characterization of such surfaces is very difficult experimentally and therefore atomistic simulation can provide unique insight and can be used to predict how a template might facilitate particular (reactive) surfaces as we have shown in this present study.

Our simulations reveal, for mesoporous ceria (models) generated without template, that crystallization initiates at the (internal pore) surfaces of the ceria. In particular the embryonic structure of the seed exposes {111} at the surface and nucleates crystallization down into the bulk of the mesoporous architecture.[29] Conversely, for the templated ceria, the confined and amorphous environment imposed by the template prevents the evolution of nucleating seeds, which expose {111} at the internal surfaces (ceria/silica interface); rather crystallization is constrained to initiate within the "bulk" regions of the mesoporous ceria and propagates toward the surface. As the crystallization front reaches the silica template (ceria/silica interface), the confining influence of the template continues to inhibit the formation of thermodynamically stable, yet chemically unreactive, {111} surfaces; rather disordered and chemically reactive surfaces evolve.

The influence of the template is therefore pivotal and if simulation is to generate models that reflect real materials and predict their properties, then we propose that the most rational way of generating the models is to simulate each step in the experimental protocol.

Simulations presented here reveal, at the atomic level, the mechanism of how a template can perturb the embryonic stages of crystallization and how such perturbation proffers new internal surface morphologies with chemical reactivities that are potentially tunable via suitable choice of (soft, hard, or bioinspired) templating material. Moreover, simulation can provide an atomistic description of the internal surfaces of the resulting mesoporous material, which is, presently, very difficult experimentally. Such information is crucial because the surface structure is central to the reactivity of a porous ceramic.

CONCLUSIONS

Atomistic models of mesoporous ceria, which include the hierarchical structural complexity associated with the real material, have been generated by simulating each step in the synthetic protocol. Specifically, we have simulated the templated crystallization of mesoporous ceria using silica scaffolds. Our calculations reveal that templated mesoporous ceria is more reactive compared to mesoporous ceria generated without template because the silica template confines the crystallization of the (infused) ceria within its pore network, prohibiting the evolution of thermodynamically stable, yet less reactive CeO_2{111} surfaces. Instead, highly reactive "curved" surfaces evolve as the infused ceria adopts the morphology of the interconnecting pore network of the silica template. The strategy affords a general method for generating atomistic models of mesoporous materials, which can be used to predict a variety of properties enabling the nanoscale design of functional materials.

AUTHOR INFORMATION

Corresponding Author

d.c.sayle@kent.ac.uk

Notes

The authors declare no competing financial interest.

ACKNOWLEDGMENTS

EP/H001220/1 and S. Hall for valuable discussion.

REFERENCES

(1) Walker, D. A.; Kowalczyk, B.; de la Cruz, M. O.; Grzybowski, B. A. *Nanoscale* **2011**, *3*, 1316−1344.
(2) Tan, J. P. Y.; Tan, H. R.; Boothroyd, C.; Foo, Y. L.; He, C. B.; Lin, M. *J. Phys.Chem. C* **2011**, *115*, 3544−3551.
(3) Li, D. S.; Nielsen, M. H.; Lee, J. R. I.; Frandsen, C.; Banfield, J. F.; De Yoreo, J. J. *Science* **2012**, *336*, 1014−1018.
(4) Green, D. C.; Glatzel, S.; Collins, A. M.; Patil, A. J.; Hall, S. R. *Adv. Mater.* **2012**, *24*, 5767−5772.
(5) Rudisill, S. G.; Wang, Z.; Stein, A. *Langmuir* **2012**, *28*, 7310−7324.
(6) Gale, J. D. *Z. Kristallogr.* **2005**, *220*, 552−554.
(7) Sayle, D. C.; Sayle, T. X. T. *Catalytic Science Series* **2013**, *12*, 2nd Edition, 247-294. ISBN: 978-1-84816-965-4 (ebook).
(8) Sayle, D. C.; Seal, S.; Wang, Z.; Mangili, B. C.; Price, D. W.; Karakoti, A. S.; Kuchibhatla, S. V. T. N.; Hao, Q.; Mobus, G.; Xu, X.; Sayle, T. X. T. *ACS Nano* **2008**, *2*, 1237−1251.
(9) Ji, P. F.; Zhang, J. L.; Chen, F.; Anpo, M. *J. Phys. Chem. C.* **2008**, *112*, 17809−17813.
(10) Mai, H. X.; Sun, L. D.; Zhang, Y. W.; Si, R.; Feng, W.; Zhang, H. P.; Liu, H. C.; Yan, C. H. *J. Phys. Chem. B.* **2005**, *109*, 24380−24385.
(11) Zhang, J.; Kumagai, H.; Yamamura, K.; Ohara, S.; Takami, S.; Morikawa, A.; Shinjoh, H.; Kaneko, K.; Adschiri, T.; Suda, A. *Nano Lett.* **2011**, *11*, 361−364.
(12) Liu, X. W.; Zhou, K. B.; Wang, L.; Wang, B. Y.; Li, Y. D. *J. Am. Chem. Soc.* **2009**, *131*, 3140−3141.
(13) Sayle, T. X. T.; Parker, S. C.; Catlow, C. R. A. *Surf. Sci.* **1994**, *316*, 329−336.
(14) Conesa, J. C. *Surf. Sci.* **1995**, *339*, 337−352.
(15) Das, S.; Singh, S.; Dowding, J. M.; Oommen, S.; Kumar, A.; Sayle, T. X. T.; Saraf, S.; Patra, C. R.; Vlahakis, N. E.; Sayle, D. C.; Self, W. T.; Seal, S. *Biomaterials* **2012**, *33*, 7746−7755.
(16) Karakoti, A. S.; Singh, S.; Kumar, A.; Malinska, M.; Kuchibhatla, S. V. N. T.; Wozniak, K.; Self, W. T.; Seal, S. *J. Am. Chem. Soc.* **2009**, *131*, 14144−14145.
(17) Stark, W. J. *Angew. Chem., Int. Ed.* **2011**, *50*, 1242−1258.
(18) Pergolesi, D.; Fabbri, E.; Cook, S. N.; Roddatis, V.; Traversa, E.; Kilner, J. A. *ACS Nano* **2012**, *6*, 10524−10534.
(19) Andersson, D. A.; Simak, S. I.; Skorodumova, N. V.; Abrikosov, I. A.; Johansson, B. *Proc. Natl. Acad. Sci. U.S.A.* **2006**, *103*, 3518−3521.

(20) Fisher, C. A. J.; Matsubara, H. *J. Eur. Ceram. Soc.* **1999**, *19*, 703−707.
(21) Adepalli, K. K.; Kelsch, M.; Rotraut Merkle, R.; Maier, J. *Adv. Funct. Mater.* **2013**, *23*, 1798−1806.
(22) Sayle, T. X. T.; Cantoni, M.; Bhatta, U. M.; Parker, S. C.; Hall, S. R.; Mobus, G.; Molinari, M.; Reid, D.; Seal, S.; Sayle, D. C. *Chem. Mater.* **2012**, *24*, 1811−1821.
(23) Smith, A. M.; Mohs, A. M.; Nie, S. *Nat. Nanotechnol.* **2009**, *4*, 56−63.
(24) Sayle, T. X. T.; Parker, S. C.; Sayle, D. C. *J. Mater. Chem.* **2006**, *16*, 1067−1081.
(25) Sun, C.; Li, H.; Chen, L. *Energy Environ. Sci.* **2012**, *5*, 8475−8505.
(26) Jackson, R. A.; Catlow, C. R. A. *Mol. Sim.* **1988**, *1*, 207−U27.
(27) Smith, W.; Forester, T. R. DL_POLY, copyright by the council for the Central Laboratory of the Research Councils; Daresbury Laboratory: Daresbury, Warrington, UK, 1996; www.cse.clrc.ac.uk/msi/software/DL_POLY/.
(28) Wang, L. Z.; Shao, Y. F.; Zhang, J. L. *Mater. Lett.* **2005**, *59*, 3604−3607.
(29) Sayle, D. C.; Feng, X.; Ding, Y.; Wang, Z.; Sayle, T. X. T. *J. Am. Chem. Soc.* **2007**, *129*, 7924−7935.
(30) Sayle, D. C.; Watson, G. W. *J. Phys. Chem. B* **2002**, *106*, 3778−3787.
(31) Sata, N.; Eberman, K.; Eberl, K.; Maier, J. *Nature* **2000**, *408*, 946−949.